

Electron and proton energization in 3D reconnecting current sheets in semirelativistic plasma with guide magnetic field

GREGORY R. WERNER¹ AND DMITRI A. UZDENSKY¹

¹ *Center for Integrated Plasma Studies, Physics Department,
390 UCB, University of Colorado, Boulder, CO 80309, USA*

ABSTRACT

Using 3D particle-in-cell simulation, we characterize energy conversion, as a function of guide magnetic field, in a thin current sheet in semirelativistic plasma, with relativistic electrons and subrelativistic protons. There, magnetic reconnection, the drift-kink instability (DKI), and the flux-rope kink instability all compete and interact in their nonlinear stages to convert magnetic energy to plasma energy. We compare fully 3D simulations with 2D in two different planes to isolate reconnection and DKI effects. In zero guide field, these processes yield distinct energy conversion signatures: ions gain more energy than electrons in 2D xy (reconnection), while the opposite is true in 2D yz (DKI), and the 3D result falls in between. The flux-rope instability, which occurs only in 3D, allows more magnetic energy to be released than in 2D, but the rate of energy conversion in 3D tends to be lower. Increasing the guide magnetic field strongly suppresses DKI, and in all cases slows and reduces the overall amount of energy conversion; it also favors electron energization through a process by which energy is first stored in the motional electric field of flux ropes before energizing particles. Understanding the evolution of the energy partition thus provides insight into the role of various plasma processes, and is important for modeling radiation from astrophysical sources such as accreting black holes and their jets.

Keywords: magnetic reconnection — plasmas — acceleration of particles

1. INTRODUCTION

In many plasma environments, magnetic energy is converted to plasma energy at thin current sheets (CSs), likely via magnetic reconnection (e.g., Zweibel & Yamada 2009). Reconnection occurs in diverse regimes and, even in 2D, generates such complexity that we owe much of our understanding to numerical simulation. Unfortunately, 3D simulation studies are far costlier than 2D, motivating efforts to understand similarities between 2D and 3D reconnection and more generally to understand 3D CS evolution in terms of 2D processes whenever possible.

A thin CS, considered in 2D [specifically in “2D xy ”, the x - y plane perpendicular to the current j_z supporting a magnetic field $\hat{\mathbf{x}}B_0\tanh(y/\delta)$ reversing over thickness 2δ], will typically be most unstable to tearing, leading, in its nonlinear stage, to reconnection and rapid magnetic energy release. In 2D yz , the same CS may kink or ripple due to the drift-kink instability (DKI), which in its nonlinear stage induces severe contortions that rapidly release magnetic energy (e.g., Pritchett et al. 1996). The DKI requires two counter-drifting species, hence is not a magnetohydrodynamics (MHD) instability; it is important when the separation between electron and ion scales is small (Daughton 1999; Hesse & Birn 2000; Scholer et al. 2003), or absent as in relativistic pair plasma (Zenitani & Hoshino 2005, 2008; Yin et al. 2008; Liu et al. 2011; Cerutti et al. 2014; Guo et al. 2014, 2015). In 3D, these instabilities can compete and interact. Although 2D-like reconnection may dominate DKI in 3D (Kagan et al. 2013; Sironi & Spitkovsky 2014; Guo et al. 2014, 2015; Cerutti et al. 2014; Werner & Uzdensky 2017; Guo et al. 2021), Werner & Uzdensky (2021) highlighted how the DKI can dramatically slow reconnection. Furthermore, in 3D only, flux ropes formed by reconnection can

decay via the MHD kink instability (Kagan et al. 2013; Markidis et al. 2014; Zhang et al. 2021b; Schoeffler et al. 2023), releasing additional magnetic energy (Werner & Uzdensky 2021).

Using particle-in-cell (PIC) simulation, this work characterizes energy conversion as a function of guide magnetic field, in 3D CSs in magnetically-dominated, collisionless electron-proton plasma, with true mass ratio $\mu = 1836$, in the semirelativistic regime. In semirelativistic plasma, where electrons are ultrarelativistic and protons subrelativistic, relativistic effects diminish the scale separation between (e.g., gyroradii of) electrons and ions (protons), making DKI consequential. The semirelativistic regime is one of the several important regimes for black hole (BH) accretion flows, which are expected to have electron-ion plasma at temperatures around 10–100MeV (e.g., Dexter et al. 2020) and likely develop large, complicated, turbulent magnetic field structures in the accretion flow, in the overlying corona/wind, and in and around the jet (e.g., Galeev et al. 1979; Uzdensky & Goodman 2008; Ripperda et al. 2020; Chashkina et al. 2021; Bacchini et al. 2022; Zhdankin et al. 2023). We generally expect CS formation and reconnection in such contexts, and the resulting particle energization could potentially power flaring emission in BHs (as in solar flares). Furthermore, characterizing electron and ion energization in the semirelativistic regime is crucial for global MHD modeling of reconnection-powered emission from accreting BHs (Chael et al. 2018; Dexter et al. 2020; Ressler et al. 2020, 2023; Scepi et al. 2022; Hankla et al. 2022).

Until now (to our knowledge), no 3D PIC studies of electron-ion reconnection (or CS evolution) have characterized energy conversion in the nonradiative semirelativistic regime (N.B., Chernoglazov et al. 2023, includes 1% ultrarelativistic ions among positrons and electrons, with radiative cooling), although several 2D reconnection studies have (Melzani et al. 2014b,a; Guo et al. 2016; Rowan et al. 2017, 2019; Werner et al. 2018; Ball et al. 2018, 2019).

After describing the simulation setup (§2), we will focus on the different energy components, discussing the release of magnetic energy U_{Bxy} (§3), the increase in guide field energy U_{Bz} (§4), the electric field energy U_E (§5), and the electron and ion energies $U_e + U_i = U_{\text{ptcl}}$ (§6). We summarize in §7.

2. THE SIMULATIONS

Simulations were run with the ZELTRON electromagnetic PIC code (Cerutti et al. 2013), initialized with semirelativistic electron-proton plasma in a standard Harris sheet configuration with uniform background plasma (similar to Werner et al. 2018)—initial physical and numerical parameters are listed in Table 1. By “semirelativistic” we mean that ions remain subrelativistic while electrons are ultrarelativistic and experience ultrarelativistic energy gains; in terms of quantities in Table 1, $m_e c^2 \ll T_b \ll m_i c^2$ and $\sigma_i \ll 1 \ll \sigma_e$. The simulation frame (with zero initial electric field) is the zero-momentum frame, where ions drift slowly and electrons carry the current supporting the field reversal.

The initial CS is perpendicular to y , with current in the $+z$ direction and reversing magnetic field in the $\pm x$ directions (approaching value B_0 upstream). We add uniform guide field $B_{gz}\hat{z}$, exploring several strengths $B_{gz}/B_0 \in \{0, 0.25, 0.5, 1, 2, 4\}$ (except $B_{gz}/B_0 = 4$ was not run in 3D, due to expense). We also explore three dimensionalities: $2Dxy$ (2D simulation ignoring z —classic 2D reconnection), $2Dyz$ (ignoring x , for studying DKI), and full 3D. Also: in one case, $2Dyz$ and $B_{gz} = 0$, we ran an ensemble of 3 simulations, identical except for differing randomization of initial particles.

Table 2 lists length scales of interest in terms of $\sigma_i \rho_{i0} = \sigma_e \rho_{e0}$, where $\rho_{s0} \equiv m_s c^2 / (eB_0)$; $\sigma_e \rho_{e0}$ is the gyroradius of an “energized” electron with energy $2B_0^2 / (8\pi n_{be})$ in perpendicular field B_0 .

The system size, containing a single CS, is $L \equiv L_y = 55.3\sigma_i \rho_{i0}$ and $L_x = L_z = L$ [except when $B_{gz} > B_0$, we increase $L_z = (B_{gz}/B_0)L_y$; and 2D simulations lack either the x or z dimension]. Boundary conditions are periodic in x and z , and conducting/particle-reflecting in y . The size L is large with respect to initial kinetic scales and CS thickness [e.g., $L/(2\delta) = 83$], and $L > 20\sigma_i \rho_{i0}$ puts it in the “large system regime” as defined by Werner et al. (2016), albeit for relativistic pair plasma in $2Dxy$.

We empirically found that using anisotropic grid cells with $\Delta x/1.6 = \Delta y = \Delta z = \sigma_i \rho_{i0}/28$ avoids numerical instabilities while yielding the best computational performance. We similarly found that the number of computational macroparticles (each representing many physical particles) needed to avoid unphysical electron-ion energy exchange at late times was 160 per cell per species (with 4 species: background and CS electrons and ions) in 2D, whereas, in 3D, 10 macroparticles/cell/species sufficed.

No initial perturbation is used to kickstart reconnection, because such a perturbation (if uniform in z) can significantly suppress 3D effects (Werner & Uzdensky 2021). Initial instabilities are therefore seeded by macroparticle noise.

Table 1. Initial plasma and numerical simulation parameters.

$\mu \equiv m_i/m_e = 1836$	ion/electron mass ratio
B_0	asymptotic upstream (reversing) magnetic field
$n_b = n_{be} = n_{bi}$	background electron/ion density
$T_b = 18.36m_e c^2 = 0.01m_i c^2$	background electron/ion temperature
$\sigma_i \equiv B_0^2/(4\pi n_b m_i c^2) = 0.5$	background ion cold magnetization
$\sigma_e \equiv B_0^2/(4\pi n_b m_e c^2) = \mu\sigma_i = 918$	background electron cold magnetization
$\delta = 0.33\sigma_i\rho_{i0}$	Harris CS half thickness ($\rho_{i0} \equiv m_i c^2/eB_0$)
$\mathbf{B}(y) = \hat{\mathbf{z}}B_{gz} - \hat{\mathbf{x}}B_0 \tanh(y/\delta)$	magnetic field profile
$-0.6c\hat{\mathbf{z}}, +0.0004c\hat{\mathbf{z}}$	electron, ion bulk drift velocities in CS
$\eta \equiv n_{d,\max}/n_b = 5$	CS overdensity
$n_d(y) = \eta n_b \cosh^{-2}(y/\delta)$	CS electron/ion density profile
$T_d = 51m_e c^2 = 0.28m_i c^2$	CS electron/ion (co-moving) temperature
$\beta_{be} = \beta_{bi} \equiv 8\pi n_b T_b/B_0^2 = 0.04$	upstream plasma beta for electrons/ions
$v_A = 0.57c$	upstream Alfvén velocity for $B_{gz} = 0$
$L_y \equiv L = 55.3\sigma_i\rho_{i0}$	system size (in y)
$L_x/L = 1$	system x/y aspect ratio (for 2D xy and 3D)
$L_z/L = \max(1, B_{gz}/B_0)$	system z/y aspect ratio (for 2D yz and 3D)
$T = 20L/c$	simulation duration
$\Delta y = \Delta z = 0.036\sigma_i\rho_{i0}$	grid cell size in y and z
$\Delta x = 0.058\sigma_i\rho_{i0}$	grid cell size in x
$\Delta t = 0.64\Delta y/c$	timestep (the 3D Courant-Friedrichs-Lewy maximum)
$M_{\text{ppcs}} = 10$ (3D), 160 (2D)	macroparticles per cell per species (4 species)
$M_{\text{ppc}} = 40$ (3D), 640 (2D)	total macroparticles per cell

Table 2. Initial length scales normalized to $\sigma_i\rho_{i0} = \sigma_e\rho_{e0}$, where $\rho_{s0} = m_s c^2/eB_0$, $\sigma_s = B_0^2/(4\pi n_{bs} m_s c^2)$

$\Delta y = \Delta z$	0.036	grid cell size in y, z
Δx	0.058	grid cell size in x
ρ_{be}	0.060	upstream electron gyroradius ($B_{gz} = 0$)
$\lambda_{De} = \lambda_{Di}$	0.14	upstream electron/ion Debye length
d_e	0.25	upstream relativistic electron skin depth
δ	0.33	CS half-thickness
ρ_{bi}	0.35	upstream ion gyroradius ($B_{gz} = 0$)
$\sigma_e\rho_{e0}$	1.0	twice the energized electron gyroradius, if all magnetic energy went to electrons
d_i	1.4	upstream nonrelativistic ion skin depth
L	55.3	system size in x, y , and z (except: if $B_{gz}/B_0 > 1$, then $L_z/L = B_{gz}/B_0$)

3. QUALITATIVE EVOLUTION AND TRANSVERSE MAGNETIC ENERGY RELEASED

Over time, transverse magnetic energy U_{Bxy} is released to other forms (U_{Bxy} excludes energy in guide field B_z , which cannot be released—see §4). Figure 1(a) shows the evolution of $U_{Bxy}(t)$ for selected simulations. Figure 1(b) shows the net loss in U_{Bxy} over $T = 20L/c$ as a function of B_{gz} , for all simulations (large symbols). Ultimately this energy ΔU_{Bxy} goes almost entirely to particles (ΔU_{ptcl} , small symbols; cf. §6), with the small difference $|\Delta U_{Bxy}| - \Delta U_{\text{ptcl}}$ comprising mainly ΔU_{Bz} , the increase in guide-field energy (see §4).

In 2D xy (Fig. 1a, blue triangles), magnetic energy decreases rapidly due to magnetic reconnection until saturation after 5–10 L/c . During that time we observe the familiar behavior of plasmoid-dominated reconnection. Reconnection pumps magnetic energy and flux from the upstream into plasmoids (magnetic islands), continually growing the total plasmoid volume and the magnetic energy therein. Apart from merging, plasmoids are permanent (stable) in 2D. Eventually (after 5–10 L/c), in a closed system, the largest plasmoid becomes so large ($\sim L$) that it halts reconnection—even though considerable transverse magnetic energy may remain upstream as well as in the plasmoid.

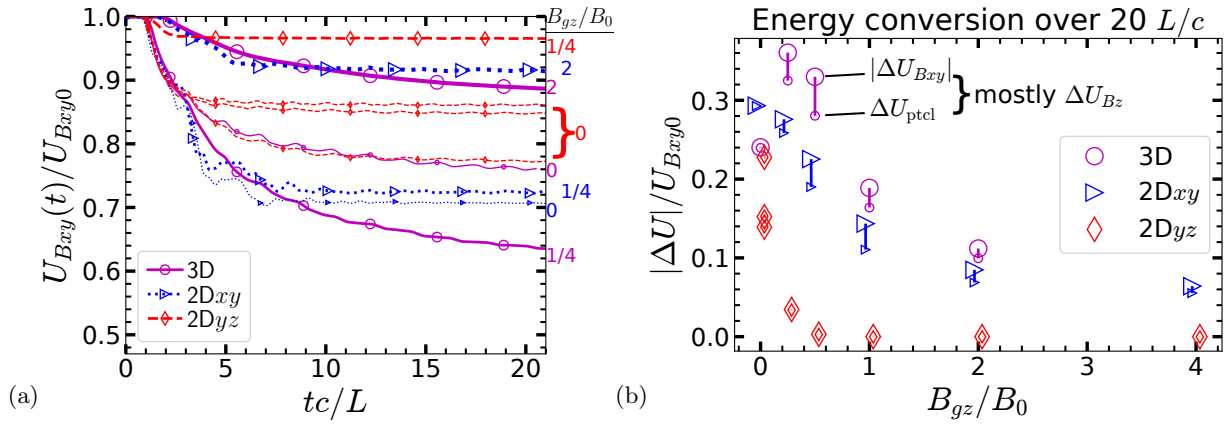


Figure 1. (a) $U_{Bxy}(t)$ for selected simulations (B_{gz} is labeled for each). Three (differently-seeded) 2Dyz simulations with $B_{gz} = 0$ demonstrate the enhanced stochastic variability of DKI. (b) $|\Delta U_{Bxy}|$ (large symbols) and ΔU_{ptcl} (small symbols) versus B_{gz} , normalized to U_{Bxy0} , the initial transverse magnetic energy.

In 2Dyz (Fig. 1, red diamonds), tearing and reconnection are forbidden, but the nonlinear DKI can rapidly release magnetic energy. We observe qualitatively similar behavior—the rippling of the CS, sometimes leading to a catastrophic folding-over on itself—as reported in nonrelativistic electron-ion plasma with artificially low m_i/m_e and in relativistic pair plasma (Ozaki et al. 1996; Pritchett & Coroniti 1996; Pritchett et al. 1996; Zhu & Winglee 1996; Zenitani & Hoshino 2007; Cerutti et al. 2014; Werner & Uzdensky 2021). The nonlinear DKI effectively thickens the CS, significantly slowing but not fully halting energy conversion. A DKI mode may enter the nonlinear stage when its rippling amplitude exceeds its rippling wavelength, but—like waves breaking in the ocean—whether and where this occurs has a substantial element of randomness (see Figs. 28, 29, 35, in Werner & Uzdensky 2021). While a large statistical study is beyond the scope of this work, this stochastic variation is shown via the three 2Dyz simulations with $B_{gz} = 0$ (red diamonds and thin dashed lines) in Fig. 1(a).

In 3D (Fig. 1, magenta circles), U_{Bxy} can be released by reconnection *and* DKI. In addition, flux ropes (3D plasmoids) formed by reconnection may decay via the flux-rope kink instability, releasing still more magnetic energy than in 2D (Fig. 1b). Because kinking flux ropes decay, reconnection will not halt as in 2Dxy, although CS thickening (due to DKI and flux-rope instability) slows both DKI and reconnection; all the 3D simulations in Fig. 1(a) show continued but slow energy conversion beyond $20 L/c$ (Werner & Uzdensky 2021).

In Fig. 1(b) we see that, for $B_{gz} = 0$, all dimensionalities yield comparable $|\Delta U_{Bxy}| \sim 0.2\text{--}0.3U_{Bxy0}$. While a small guide field $B_{gz}/B_0 = 1/4$ has only a small effect in 2Dxy and 3D, it strongly inhibits energy conversion in 2Dyz (Zenitani & Hoshino 2008).

Increasing B_{gz} has two main effects, in all cases: it slows energy conversion, and decreases the net magnetic energy release $|\Delta U_{Bxy}|$. A guide field of $B_{gz}/B_0 \gtrsim 1/2$ stabilizes the DKI in 2Dyz (cf. Zenitani & Hoshino 2008; Schoeffler et al. 2023), preventing any release of U_{Bxy} . For 2Dxy and 3D, increasing B_{gz}/B_0 from 0 to 1 slows energy conversion and reduces $|\Delta U_{Bxy}|$ by roughly half; by $B_{gz}/B_0 = 2$, only about $0.1U_{Bxy0}$ is released (this depends on the aspect ratio: for $L_y \gtrsim L_x$, we expect $|\Delta U_{Bxy}|/U_{Bxy0} \sim 0.1L_x/L_y$). Previous 2Dxy studies showed that B_{gz} slows reconnection by reducing the Alfvén speed $v_{A,x}$ in the outflow direction (Liu et al. 2014; Werner & Uzdensky 2017); also, B_{gz} resists plasmoid compression, halting reconnection at smaller $|\Delta U_{Bxy}|$. These trends hold in 3D as well, except that increasing B_{gz}/B_0 from 0 to 1/4 releases more energy, possibly because B_z suppresses the DKI and prevents interference with reconnection, or possibly this is stochastic variation; we leave exploration of this subtrend to future work.

Overall, after $20 L/c$, ΔU_{Bxy} is about 15% higher in 3D than in 2Dxy because 3D evolution accesses all the 2D dissipation channels plus the flux-rope instability; the difference between 2Dxy and 3D narrows slightly with higher B_{gz} as guide field increases uniformity in z . We note that with more time, $|\Delta U_{Bxy}|$ would increase in 3D, but not in 2Dxy.

4. ENERGY GAIN IN GUIDE FIELD

In our simulations, the guide-field energy U_{Bz} can only increase from its initial value; the B_z -flux through any x - y plane is conserved and B_z is initially uniform, yielding the lowest U_{Bz} for the fixed flux. Figure 2(a) shows the net gain ΔU_{Bz} versus B_{gz} for each dimensionality. In the 2Dyz case, $\Delta U_{Bz} \approx 0$, and for $B_{gz} = 0$ neither 2Dxy nor 3D show noticeable gain. However, for $B_{gz} > 0$, reconnection outflows compress plasma *and* guide field in flux ropes,

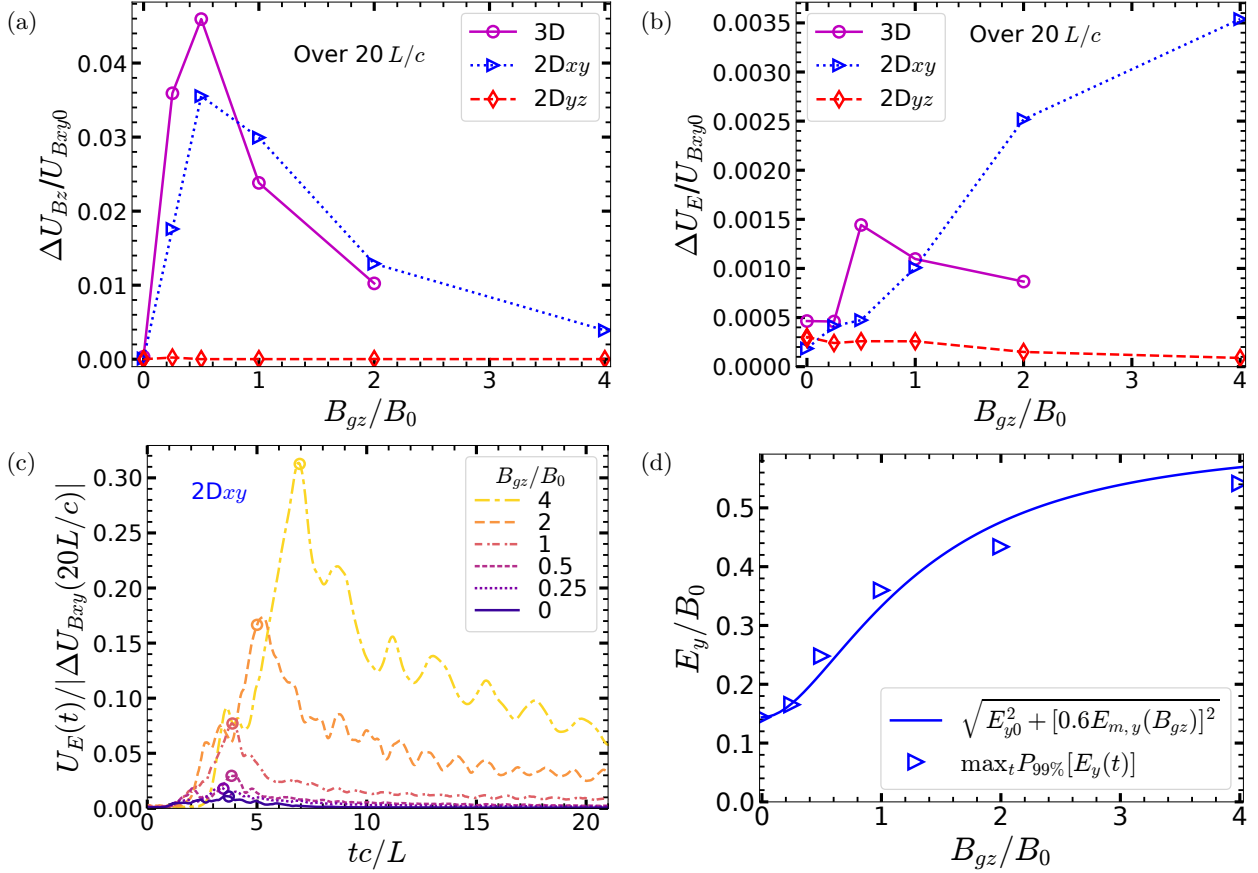


Figure 2. (a) Net gain in U_{Bz} versus B_{gz} , in 2Dxy (blue triangles), 3D (magenta circles), and 2Dyz (red diamonds showing zero gain). (b) Net gain in $U_E(B_{gz})$. (c) For 2Dxy only, $U_E(t)$ vs. time, for different B_{gz} , normalized to the ultimately-released magnetic energy [not shown: in 2Dyz and 3D, $U_E(t)$ remains relatively small]. U_E dissipates only after most of U_{Bxy} has dissipated, as indicated by the circles placed where $\Delta U_{Bxy}(t) = 0.75\Delta U_{Bxy}(20L/c)$. (d) For 2Dxy, the plasmoid E_y as a function of B_{gz} , estimated from Eqs. (1)–(2) (solid line), compared with the maximum E_y measured in simulations (triangles). (To reduce sensitivity to noise, the maximum was measured over time of the 99th percentile of $|E_y|$.)

increasing U_{Bz} . The gain ΔU_{Bz} increases with $B_{gz}/B_0 \lesssim 0.5$ because there is more B_z to be compressed; however, stronger B_{gz} rivals the plasma in resisting compression (with adiabatic index 2, greater than the adiabatic index 4/3 or 5/3 of relativistic or nonrelativistic plasma; cf. §4.4 of Werner & Uzdensky 2021), and ΔU_{Bz} peaks around $0.04 U_{Bxy0}$ at $B_{gz}/B_0 \sim 0.5$ before decreasing. The similarity between 2Dxy and 3D suggests reconnection occurs to similar extents—though slower in 3D—resulting in similar compression of flux ropes, with energy remaining in U_{Bz} even as flux ropes decay in 3D.

We note that the contribution of the Hall quadrupole B_z field is negligible on global energy scales, because it is localized to small regions around X-lines; in contrast, the U_{Bz} in plasmoids becomes globally significant because it grows with plasmoids, which approach the system size.

5. ENERGY GAIN AND SUBSEQUENT LOSS IN ELECTRIC FIELD

The net gain in electric field energy U_E is negligible in all cases—less than $0.004 U_{Bxy0}$ (Fig. 2b). For 2Dyz and 3D, $U_E(t)$ is small at all times. However (see Fig. 2c), in 2Dxy with strong guide field, $U_E(t)$ builds up substantially over time before declining (after most reconnection has occurred); this effect increases with B_{gz} . For $B_{gz}/B_0 = 2$, 17% of the ultimately-released magnetic energy resided *at one time* (around $t = 5L/c$) in U_E , and for $B_{gz}/B_0 = 4$, over 30%.

This effect—by which substantial U_{Bxy} is first converted to U_E before energizing particles—has not been reported before, to our knowledge. We find that (when $B_{gz}/B_0 \gtrsim 0.5$) U_E is dominated by E_y in plasmoids; this is simply the motional electric field $E_{m,y} \approx v_x B_z/c$ due to B_z in a plasmoid moving with relativistic speed v_x along the layer. This effect should appear in any 2D reconnection simulation with guide field and relativistic outflows, even in pair plasma.

After the last major plasmoid merger, as reconnection is ending, only one large but stationary plasmoid remains, and thus the motional electric field ultimately decays.

We can estimate how $E_{m,y} \approx v_x B_z / c$ scales with guide field, assuming that $B_z \sim B_{gz}$ and that plasmoid velocity v_x scales with $v_{A,x}$, the Alfvén velocity projected along x . Since the typical reconnection electric field is $E_{\text{rec}} \sim 0.1 v_{A,x} B_0 / c$ (for fast collisionless reconnection), $E_{m,y} / E_{\text{rec}} \sim 10 B_{gz} / B_0$, which exceeds unity for even small B_{gz} . In absolute terms, $v_{A,x} = c [B_0^2 / (4\pi h + B_0^2 + B_{gz}^2)]^{1/2}$, where h is the relativistic plasma enthalpy density including rest-mass (Liu et al. 2014; Sironi et al. 2016; Werner & Uzdensky 2017), and thus

$$E_{m,y}(B_{gz}) \sim \sqrt{\frac{B_{gz}^2 B_0^2}{4\pi h + B_0^2 + B_{gz}^2}} \rightarrow \begin{cases} E_{m,y} \propto B_{gz} & \text{for } B_{gz}^2 \ll B_0^2 + 4\pi h \\ E_{m,y} \sim B_0 & \text{for } B_{gz}^2 \gtrsim B_0^2 + 4\pi h \end{cases}. \quad (1)$$

(In this paper, $4\pi h \approx 4\pi n_b m_i c^2 = B_0^2 / \sigma_i = 2B_0^2$.)

This estimate of $E_{m,y}(B_{gz})$ roughly explains the B_{gz} -dependence of E_y in our 2D xy simulations; Fig. 2(d) shows the maximum observed E_y compared with

$$E_{y,\text{max}}(B_{gz}) = \sqrt{E_{y0}^2 + [\alpha E_{m,y}(B_{gz})]^2}, \quad (2)$$

which adds in quadrature the motional field $E_{m,y}(B_{gz})$ given by Eq. (1) and $E_{y0} \equiv E_{y,\text{max}}(0) \approx 0.14 B_0$, an estimate of E_y from other sources (which we measure in the simulation with $B_{gz} = 0$ and assume it remains similar for $B_{gz} > 0$), with empirical factor $\alpha \approx 0.6$ accounting for, e.g., $v_x < v_{A,x}$.

Notably, when U_E dissipates at the end of reconnection, it preferentially energizes electrons, as described next.

6. ENERGY GAIN IN ELECTRONS AND IONS

In all dimensionalities, increasing guide field generally suppresses both electron and ion energization relative to the available magnetic energy U_{Bxy0} (Fig. 3a,b). In 2D yz , both electron and ion net gains (ΔU_e and ΔU_i) drop precipitously with B_{gz} . In 2D xy and 3D, energy gains also fall, but not to zero, and ΔU_i falls much faster than ΔU_e . As B_{gz}/B_0 increases from 0.25 to 2, ΔU_e falls from $0.09 U_{Bxy0}$ to $0.05 U_{Bxy0}$ in 2D xy , and from $0.16 U_{Bxy0}$ to $0.09 U_{Bxy0}$ in 3D; in contrast, ΔU_i falls from about $0.17 U_{Bxy0}$ to just $0.02 U_{Bxy0}$ (almost an order of magnitude!), and is nearly identical in 2D xy and 3D. The additional magnetic energy released in 3D (compared with 2D xy) goes mostly to electrons. At low B_{gz} , this may be due to the DKI and/or the flux-rope kink instability; at higher B_{gz} , DKI is quenched, suggesting that the flux-rope kink preferentially energizes electrons. The electron energy gain fraction $q_e \equiv \Delta U_e / (\Delta U_e + \Delta U_i)$ grows with B_{gz} (Fig. 3c), even though ΔU_e decreases. In 2D xy , $q_e \approx 0.35$ at $B_{gz} = 0$, increasing to $q_e \approx 0.5$ (equipartition) around $B_{gz}/B_0 = 0.75$, and reaching $q_e > 0.8$ by $B_{gz}/B_0 = 4$. In 3D, $q_e(B_{gz})$ is higher than in 2D xy by about 0.1 (though this gap narrows as B_{gz} increases), reaching equipartition near $B_{gz}/B_0 = 0.25$, and $q_e \approx 0.7$ at $B_{gz}/B_0 = 1$. In 2D yz , q_e is ~ 0.2 higher than in 3D, but we emphasize that, for $B_{gz}/B_0 \geq 0.5$, ΔU_e in 2D yz is tiny compared with 2D xy and 3D (hence hard to measure).

The 3D case with $B_{gz} = 0$ is exceptional, converting less energy than higher $B_{gz}/B_0 = 0.25$, but the difference is within the stochastic variation observed in 2D yz for $B_{gz} = 0$ (cf. Figs. 1b and 3a,b).

In the following, we compare q_e previously measured in 2D xy PIC reconnection simulations in the (nearly) semirelativistic, plasmoid-dominated regime. For $B_{gz} = 0$, $q_e \simeq 0.25\text{--}0.35$ was found in similar simulations (Rowan et al. 2017, 2019; Werner et al. 2018; Zhang et al. 2021b) and also in the different regime of nonrelativistic laboratory experiment (e.g., Yamada et al. 2014). Similar increases in q_e with B_{gz} were also reported in 2D: e.g., Rowan et al. (2019) found q_e increasing to equipartition around $B_{gz}/B_0 \approx 1$ and up to 0.92 for $B_{gz}/B_0 = 6$; with reduced mass ratio $\mu = 25$, Melzani et al. (2014a) found q_e increasing to 0.67 at $B_{gz}/B_0 = 1$. There have, however, been no 3D PIC simulations in a quantitatively comparable regime (to our knowledge) that have measured q_e .

Although a detailed analysis of energization mechanisms is beyond the scope of this Letter, the time-dependence of q_e offers some insight. Figure 3(d) plots q_e separately for each third (in terms of ΔU_{Bxy} , not time) of each simulation. In 2D yz , we observe no significant time-dependence of q_e . For 2D xy and strong B_{gz} , however, the last third (when U_E dissipates; see Fig. 2c) has much higher q_e than the first two thirds. Therefore, we conclude that energization by the motional electric field $E_{m,y}$ differs from reconnection energization mechanisms that operate earlier (or without B_{gz}), and yields higher q_e . In 3D, for strong B_{gz} , we see the last two-thirds have higher q_e than the first third, suggesting that U_E builds up a little in 3D, but is promptly dissipated. That is, energization-via- $E_{m,y}$ operates continuously throughout 3D reconnection, but only at the end of 2D xy reconnection due to the high integrity of plasmoids. Besides being useful in their own right, measurements of q_e can thus help distinguish between different energization mechanisms.

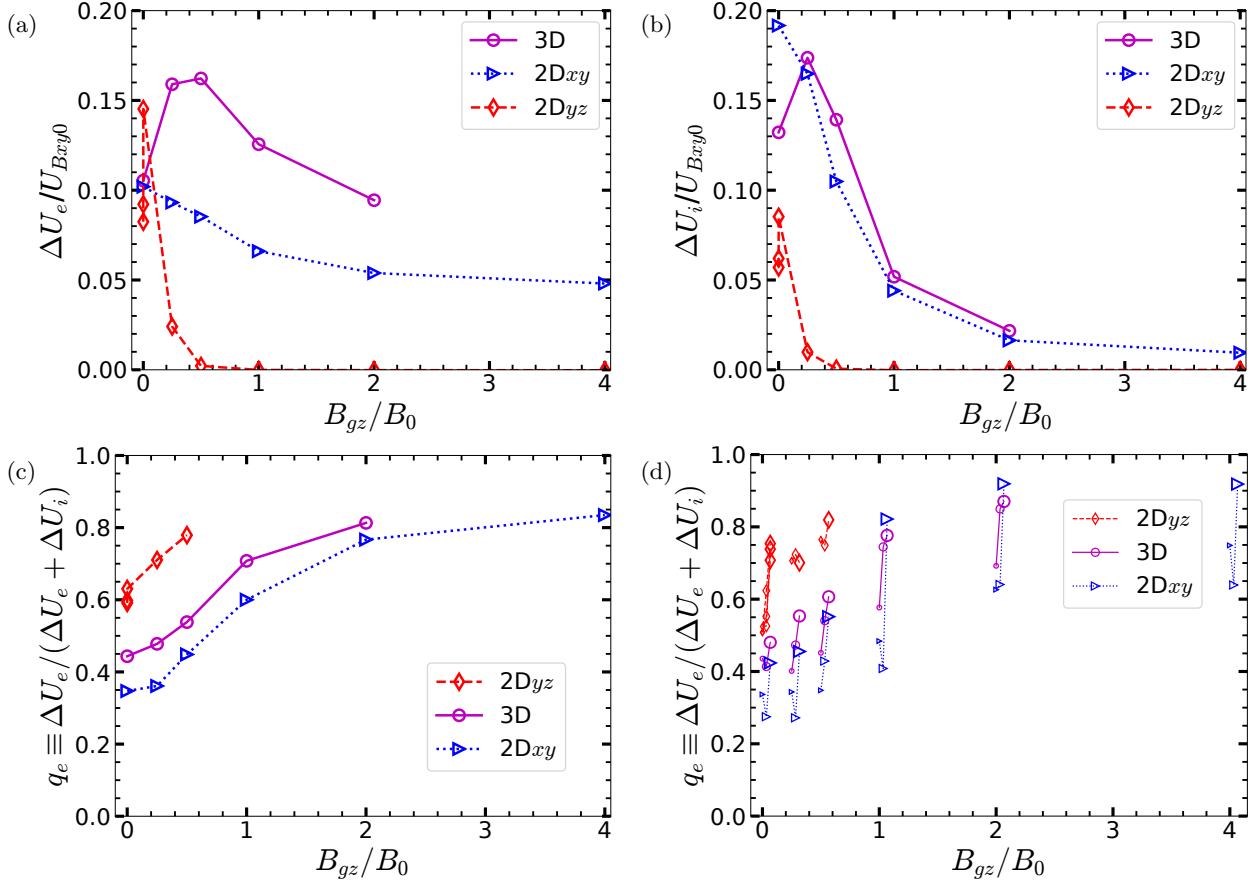


Figure 3. The net gain in (a) electron and (b) ion energy, versus B_{gz} , normalized by initial transverse magnetic energy U_{Bxy0} , over the full $T = 20 L/c$. (c) The electron gain fraction q_e versus B_{gz} . (d) q_e for each third (in terms of ΔU_{Bxy}) of each simulation (the smallest markers, shifted left, show q_e in the first third; the largest, shifted right, show the last third). 2Dyz cases with $B_{gz}/B_0 > 0.5$, hence negligible energization, are omitted.

7. SUMMARY

Using PIC simulation, we evolve a thin current sheet in 3D semirelativistic plasma (see Table 1), investigating energy conversion for different guide magnetic fields B_{gz} . The 3D simulations are compared with 2Dxy (reconnection) and 2Dyz (drift-kink) simulations with the same initial conditions.

We quantify the net changes in transverse and guide magnetic, electric, electron kinetic, and ion kinetic energies. We find:

- Increasing B_{gz} slows energy conversion and reduces the total released magnetic energy.
- Increasing B_{gz} suppresses ion energization more than electron energization, increasing $q_e \equiv \Delta U_e/(\Delta U_e + \Delta U_i)$. In 3D, $\Delta U_e/U_{Bxy0}$ falls from 0.16 to 0.09 as B_{gz}/B_0 increases from 0.25 to 2, while $\Delta U_i/U_{Bxy0}$ falls from 0.17 to 0.02; q_e rises from roughly 0.5 to 0.8.
- In 3D only, the flux-rope kink instability further energizes particles (mostly electrons), releasing the reconnected transverse magnetic energy stored in flux ropes, but not their guide-field energy (which is increased by compression during reconnection).
- Relativistic reconnection in strong guide field transfers energy to transient motional electric fields $E_{m,y}$ in flux ropes before preferentially energizing electrons. In 2Dxy, U_E grows substantially, and dissipates only at the end of reconnection; in 3D, U_E dissipates promptly, possibly due to flux-rope decay.
- Different plasma processes operating in thin CSs yield different electron/ion energy partitions. We roughly distinguished electron energy fractions q_e due to four mechanisms: DKI, classic 2D reconnection, dissipation

of $E_{m,y}$, and flux-rope kink instability. Their relative roles (especially for DKI and reconnection) in 3D may be sensitive to the CS configuration.

We have thus characterized the conversion of magnetic energy to electron and ion kinetic energy in 3D CSs, addressing a fundamental plasma-physics question and obtaining new insight into the interplay of multiple dissipation channels yielding different energization of electrons versus ions. Importantly, we measured, from first-principles simulation, electron and ion heating fractions critical for subgrid modeling of electron energization (e.g., Dexter et al. 2020; Scepi et al. 2022), and we showed that they depend significantly on the guide magnetic field. These results, in combination with similar studies in the 3D relativistic pair-plasma regime (e.g., Zenitani & Hoshino 2008; Yin et al. 2008; Liu et al. 2011; Kagan et al. 2013; Cerutti et al. 2014; Guo et al. 2014; Guo et al. 2021; Sironi & Spitkovsky 2014; Werner & Uzdensky 2017; Werner & Uzdensky 2021; Zhang et al. 2021a), will be important in connecting magnetic energy dissipation with particle energization and observed radiation in the complex and varied environment of accreting BHs.

This work was supported by NSF grants AST-1806084 and AST-1903335 and by NASA grants 80NSSC20K0545 and 80NSSC22K0828. The 3D simulations used computer time provided by the U.S. Department of Energy’s (DOE) Innovative and Novel Computational Impact on Theory and Experiment (INCITE) Program, and in particular used resources from the Argonne Leadership Computing Facility, a U.S. DOE Office of Science user facility at Argonne National Laboratory, which is supported by the Office of Science of the U.S. DOE under Contract No. DE-AC02-06CH11357. The 2D simulations were run on the Frontera supercomputer at the Texas Advanced Computing Center (TACC) at The University of Texas at Austin.

REFERENCES

- Bacchini F, Arzamasskiy L, Zhdankin V, Werner GR, Begelman MC, & Uzdensky DA, **2022**, “Fully Kinetic Shearing-box Simulations of Magnetorotational Turbulence in 2D and 3D. I. Pair Plasmas,” *ApJ*, 938(1), 86. DOI:10.3847/1538-4357/ac8a94 arXiv:2206.07061
- Ball D, Sironi L, & Özel F, **2018**, “Electron and Proton Acceleration in Trans-relativistic Magnetic Reconnection: Dependence on Plasma Beta and Magnetization,” *ApJ*, 862(1), 80. DOI:10.3847/1538-4357/aac820 arXiv:1803.05556
- Ball D, Sironi L, & Özel F, **2019**, “The Mechanism of Electron Injection and Acceleration in Transrelativistic Reconnection,” *ApJ*, 884(1), 57. DOI:10.3847/1538-4357/ab3f2e arXiv:1908.05866
- Cerutti B, Werner GR, Uzdensky DA, & Begelman MC, **2013**, “Simulations of Particle Acceleration beyond the Classical Synchrotron Burnoff Limit in Magnetic Reconnection: An Explanation of the Crab Flares,” *ApJ*, 770, 147. DOI:10.1088/0004-637X/770/2/147 arXiv:1302.6247
- Cerutti B, Werner GR, Uzdensky DA, & Begelman MC, **2014**, “Three-dimensional Relativistic Pair Plasma Reconnection with Radiative Feedback in the Crab Nebula,” *ApJ*, 782, 104. DOI:10.1088/0004-637X/782/2/104 arXiv:1311.2605
- Chael A, Rowan M, Narayan R, Johnson M, & Sironi L, **2018**, “The role of electron heating physics in images and variability of the Galactic Centre black hole Sagittarius A*,” *MNRAS*, 478(4), 5209–5229. DOI:10.1093/mnras/sty1261 arXiv:1804.06416
- Chashkina A, Bromberg O, & Levinson A, **2021**, “GRMHD simulations of BH activation by small scale magnetic loops: formation of striped jets and active coronae,” *MNRAS*, 508(1), 1241–1252. DOI:10.1093/mnras/stab2513 arXiv:2106.15738
- Chernoglazov A, Hakobyan H, & Philippov A, **2023**, “High-energy Radiation and Ion Acceleration in Three-dimensional Relativistic Magnetic Reconnection with Strong Synchrotron Cooling,” *ApJ*, 959(2), 122. DOI:10.3847/1538-4357/acffc6 arXiv:2305.02348
- Daughton W, **1999**, “Two-fluid theory of the drift kink instability,” *J. Geophys. Res.*, 104(A12), 28701–28708. DOI:10.1029/1999JA900388
- Dexter J, Jiménez-Rosales A, Ressler SM, Tchekhovskoy A, Bauböck M, de Zeeuw PT, Eisenhauer F, von Fellenberg S, Gao F, Genzel R, Gillessen S, Habibi M, Ott T, Stadler J, Straub O, & Widmann F, **2020**, “A parameter survey of Sgr A* radiative models from GRMHD simulations with self-consistent electron heating,” *MNRAS*, 494(3), 4168–4186. DOI:10.1093/mnras/staa922 arXiv:2004.00019

- Galeev A, Rosner R, & Vaiana G, **1979**, “Structured coronae of accretion disks,” *ApJ*, 229, 318
- Guo F, Li H, Daughton W, & Liu YH, **2014**, “Formation of hard power laws in the energetic particle spectra resulting from relativistic magnetic reconnection,” *Phys. Rev. Lett.*, 113, 155005. DOI:10.1103/PhysRevLett.113.155005
- Guo F, Li X, Daughton W, Li H, Kilian P, Liu YH, Zhang Q, & Zhang H, **2021**, “Magnetic Energy Release, Plasma Dynamics, and Particle Acceleration in Relativistic Turbulent Magnetic Reconnection,” *ApJ*, 919(2), 111. DOI:10.3847/1538-4357/ac0918 arXiv:2008.02743
- Guo F, Li X, Li H, Daughton W, Zhang B, Lloyd-Ronning N, Liu YH, Zhang H, & Deng W, **2016**, “Efficient production of high-energy nonthermal particles during reconnection in a magnetically dominated ion-electron plasma,” *ApJ Lett.*, 818(1), L9
- Guo F, Liu YH, Daughton W, & Li H, **2015**, “Particle acceleration and plasma dynamics during magnetic reconnection in the magnetically dominated regime,” *ApJ*, 806(2), 167
- Hankla AM, Scepi N, & Dexter J, **2022**, “Non-thermal emission from the plunging region: a model for the high-energy tail of black hole X-ray binary soft states,” *MNRAS*, 515(1), 775–784. DOI:10.1093/mnras/stac1785 arXiv:2206.12018
- Hesse M, & Birn J, **2000**, “Near- and Mid-tail Current Flow During Substorms: Small- and Large-Scale Aspects of Current Disruption,” *Geophysical Monograph Series*, 118, 295. DOI:10.1029/GM118p0295
- Kagan D, Milosavljević M, & Spitkovsky A, **2013**, “A Flux Rope Network and Particle Acceleration in Three-dimensional Relativistic Magnetic Reconnection,” *ApJ*, 774, 41. DOI:10.1088/0004-637X/774/1/41 arXiv:1208.0849
- Liu W, Li H, Yin L, Albright BJ, Bowers KJ, & Liang EP, **2011**, “Particle energization in 3D magnetic reconnection of relativistic pair plasmas,” *Physics of Plasmas*, 18(5), 052105. DOI:10.1063/1.3589304 arXiv:1005.2435
- Liu YH, Daughton W, Karimabadi H, Li H, & Peter Gary S, **2014**, “Do dispersive waves play a role in collisionless magnetic reconnection?,” *Phys. Plasmas*, 21(2), 022113. DOI:10.1063/1.4865579
- Markidis S, Lapenta G, Delzanno GL, Henri P, Goldman MV, Newman DL, Intrator T, & Laure E, **2014**, “Signatures of secondary collisionless magnetic reconnection driven by kink instability of a flux rope,” *Plasma Phys. Contr. F.*, 56(6), 064010. DOI:10.1088/0741-3335/56/6/064010 arXiv:1408.1144
- Melzani M, Walder R, Folini D, Winisdoerffer C, & Favre JM, **2014a**, “The energetics of relativistic magnetic reconnection: ion-electron repartition and particle distribution hardness,” *Astron. Astrophys.*, 570, A112
- Melzani M, Walder R, Folini D, Winisdoerffer C, & Favre JM, **2014b**, “Relativistic magnetic reconnection in collisionless ion-electron plasmas explored with particle-in-cell simulations,” *Astron. Astrophys.*, 570, A111
- Ozaki M, Sato T, Horiuchi R, & Complexity Simulation Group, **1996**, “Electromagnetic instability and anomalous resistivity in a magnetic neutral sheet,” *Phys. Plasmas*, 3(6), 2265–2274. DOI:10.1063/1.871908
- Pritchett PL, & Coroniti FV, **1996**, “The Role of the Drift Kink Mode in Destabilizing Thin Current Sheets,” *J. Geomagn. Geoelectr.*, 48(5), 833–844. DOI:10.5636/jgg.48.833
- Pritchett PL, Coroniti FV, & Decyk VK, **1996**, “Three-dimensional stability of thin quasi-neutral current sheets,” *J. Geophys. Res.*, 101(A12), 27413–27430. DOI:10.1029/96JA02665
- Ressler SM, White CJ, & Quataert E, **2023**, “Wind-fed GRMHD simulations of Sagittarius A*: tilt and alignment of jets and accretion discs, electron thermodynamics, and multiscale modelling of the rotation measure,” *MNRAS*, 521(3), 4277–4298. DOI:10.1093/mnras/stad837
- Ressler SM, White CJ, Quataert E, & Stone JM, **2020**, “Ab Initio Horizon-scale Simulations of Magnetically Arrested Accretion in Sagittarius A* Fed by Stellar Winds,” *ApJ Lett.*, 896(1), L6. DOI:10.3847/2041-8213/ab9532 arXiv:2006.00005
- Ripperda B, Bacchini F, & Philippov AA, **2020**, “Magnetic Reconnection and Hot Spot Formation in Black Hole Accretion Disks,” *ApJ*, 900(2), 100. DOI:10.3847/1538-4357/ababab arXiv:2003.04330
- Rowan ME, Sironi L, & Narayan R, **2017**, “Electron and Proton Heating in Transrelativistic Magnetic Reconnection,” *ApJ*, 850(1), 29. DOI:10.3847/1538-4357/aa9380 arXiv:1708.04627
- Rowan ME, Sironi L, & Narayan R, **2019**, “Electron and Proton Heating in Transrelativistic Guide Field Reconnection,” *ApJ*, 873(1), 2. DOI:10.3847/1538-4357/ab03d7 arXiv:1901.05438
- Scepi N, Dexter J, & Begelman MC, **2022**, “Sgr A* X-ray flares from non-thermal particle acceleration in a magnetically arrested disc,” *MNRAS*, 511(3), 3536–3547. DOI:10.1093/mnras/stac337 arXiv:2107.08056

- Schoeffler KM, Grismayer T, Uzdensky D, & Silva LO, **2023**, “High-energy synchrotron flares powered by strongly radiative relativistic magnetic reconnection: 2D and 3D PIC simulations,” *MNRAS*, 523(3), 3812–3839. DOI:10.1093/mnras/stad1588 arXiv:2303.16643
- Scholer M, Sidorenko I, Jaroschek CH, Treumann RA, & Zeiler A, **2003**, “Onset of collisionless magnetic reconnection in thin current sheets: Three-dimensional particle simulations,” *Phys. Plasmas*, 10(9), 3521–3527. DOI:10.1063/1.1597494
- Sironi L, Giannios D, & Petropoulou M, **2016**, “Plasmoids in relativistic reconnection, from birth to adulthood: first they grow, then they go,” *MNRAS*, 462, 48–74. DOI:10.1093/mnras/stw1620 arXiv:1605.02071
- Sironi L, & Spitkovsky A, **2014**, “Relativistic Reconnection: An Efficient Source of Non-thermal Particles,” *ApJ Lett.*, 783, L21. DOI:10.1088/2041-8205/783/1/L21 arXiv:1401.5471
- Uzdensky DA, & Goodman J, **2008**, “Statistical description of a magnetized corona above a turbulent accretion disk,” *ApJ*, 682(1), 608
- Werner GR, & Uzdensky DA, **2017**, “Nonthermal Particle Acceleration in 3D Relativistic Magnetic Reconnection in Pair Plasma,” *ApJ Lett.*, 843, L27. DOI:10.3847/2041-8213/aa7892 arXiv:1705.05507
- Werner GR, & Uzdensky DA, **2021**, “Reconnection and particle acceleration in three-dimensional current sheet evolution in moderately magnetized astrophysical pair plasma,” *J. Plasma Phys.*, 87(6), 905870613. DOI:10.1017/S0022377821001185 arXiv:2106.02790
- Werner GR, Uzdensky DA, Begelman MC, Cerutti B, & Nalewajko K, **2018**, “Non-thermal particle acceleration in collisionless relativistic electron-proton reconnection,” *MNRAS*, 473, 4840–4861. DOI:10.1093/mnras/stx2530 arXiv:1612.04493
- Werner GR, Uzdensky DA, Cerutti B, Nalewajko K, & Begelman MC, **2016**, “The Extent of Power-law Energy Spectra in Collisionless Relativistic Magnetic Reconnection in Pair Plasmas,” *ApJ Lett.*, 816, L8. DOI:10.3847/2041-8205/816/1/L8 arXiv:1409.8262
- Yamada M, Yoo J, Jara-Almonte J, Ji H, Kulsrud RM, & Myers CE, **2014**, “Conversion of magnetic energy in the magnetic reconnection layer of a laboratory plasma,” *Nat. Commun.*, 5, 4774. DOI:10.1038/ncomms5774
- Yin L, Daughton W, Karimabadi H, Albright BJ, Bowers KJ, & Margulies J, **2008**, “Three-Dimensional Dynamics of Collisionless Magnetic Reconnection in Large-Scale Pair Plasmas,” *Phys. Rev. Lett.*, 101(12), 125001. DOI:10.1103/PhysRevLett.101.125001
- Zenitani S, & Hoshino M, **2005**, “Three-Dimensional Evolution of a Relativistic Current Sheet: Triggering of Magnetic Reconnection by the Guide Field,” *Phys. Rev. Lett.*, 95(9), 095001. DOI:10.1103/PhysRevLett.95.095001 arXiv:astro-ph/0505493
- Zenitani S, & Hoshino M, **2007**, “Particle Acceleration and Magnetic Dissipation in Relativistic Current Sheet of Pair Plasmas,” *ApJ*, 670, 702–726. DOI:10.1086/522226 arXiv:0708.1000
- Zenitani S, & Hoshino M, **2008**, “The Role of the Guide Field in Relativistic Pair Plasma Reconnection,” *ApJ*, 677, 530–544. DOI:10.1086/528708 arXiv:0712.2016
- Zhang H, Sironi L, & Giannios D, **2021a**, “Fast Particle Acceleration in Three-dimensional Relativistic Reconnection,” *ApJ*, 922(2), 261. DOI:10.3847/1538-4357/ac2e08 arXiv:2105.00009
- Zhang Q, Guo F, Daughton W, Li H, & Li X, **2021b**, “Efficient Nonthermal Ion and Electron Acceleration Enabled by the Flux-Rope Kink Instability in 3D Nonrelativistic Magnetic Reconnection,” *Phys. Rev. Lett.*, 127(18), 185101. DOI:10.1103/PhysRevLett.127.185101 arXiv:2105.04521
- Zhdankin V, Ripperda B, & Philippov AA, **2023**, “Particle acceleration by magnetic Rayleigh-Taylor instability: Mechanism for flares in black hole accretion flows,” *Phys. Rev. Research*, 5(4), 043023. DOI:10.1103/PhysRevResearch.5.043023 arXiv:2302.05276
- Zhu Z, & Winglee RM, **1996**, “Tearing instability, flux ropes, and the kinetic current sheet kink instability in the Earth’s magnetotail: A three-dimensional perspective from particle simulations,” *J. Geophys. Res.*, 101(A3), 4885–4898. DOI:10.1029/95JA03144
- Zweibel EG, & Yamada M, **2009**, “Magnetic Reconnection in Astrophysical and Laboratory Plasmas,” *ARA&A*, 47, 291–332. DOI:10.1146/annurev-astro-082708-101726